Structure and conformational analysis of CFC-113 by density functional theory calculations and FTIR spectroscopy

Karine Le Bris *, Kimberly Strong, Stella M.L. Melo [1], Jason C. Ng

Department of Physics, University of Toronto, 60 St. George Street, Toronto, Ont., Canada M5S 1A7

Abstract

Altitude-resolved volume mixing ratio profiles of CFC-113 have recently become available on a global scale with the Atmospheric Chemistry Experiment (ACE) satellite mission. However, the accuracy of the retrieval is currently limited by the uncertainties on the spectroscopic parameters of CFC-113. This paper reports on the geometrical structure, harmonic frequencies and intensities in the mid-infrared region of the two conformers of CFC-113 and the evaluation of whether theoretical calculations reproduce measurements. The calculations are performed using density functional theory at the B3LYP/6-311+G(3df) level. The molecular geometry parameters, the enthalpy difference and the potential barrier between conformers are calculated. The harmonic frequency of the normal modes of vibration are presented and accurately compared to experimental data. Overtones and combination bands are assigned in the 1200–2500 cm^{-1} region.

1. Introduction

CFC-113 (1,1,2-trichlorotrifluoroethane) is the third most abundant chlorofluorocarbon in the atmosphere. Its ozone depletion potential has led to its ban by the Montreal Protocol and its subsequent amendments. Although its emission is now controlled by international regulations, the long lifetime of this compound (∼85 years) makes its monitoring essential, as the average concentration of CFC-113 in the atmosphere is still approximately 80 ppt. The impact of this molecule on the ozone layer and its contribution to enhanced global warming require precise measurement of its concentration worldwide for assessing theoretical predictions and for assessment of the effective-

ness of international regulations. Recently, the Atmospheric Chemistry Experiment (ACE) satellite mission [1] has provided the first space-based atmospheric measurements of CFC-113 on a global scale [2]. However, the uncertainties in the spectroscopic parameters currently available for this molecule compromise the accuracy of the retrievals. The errors associated with spectroscopic data have been evaluated to be at least 20% [3].

Only a few attempts have been made to characterize the optical properties of CFC-113 in the vapour phase. The most recent [4], published in 1987, presented an extensive experimental study of CFC-113 in the solid, liquid and gaseous phases. An assignment of the C_1 and C_s conformers supported by a normal coordinate calculation involving related molecules was carried out. Although the comparison between theory and experiment was quite good, discrepancies existed in the 800–1250 cm^{-1} region. Because this region is of considerable interest in atmospheric science, it is crucial to verify

* Corresponding author. Fax: +1 416 978 8905.
  E-mail address: klebris@atmosp.physics.utoronto.ca (K. Le Bris).
[1] Present address: Canadian Space Agency, 6767 route de l'Aéroport, St-Hubert, Que., Canada J3Y 8Y9.

the line attribution in the vapour phase and to perform a new theoretical calculation of CFC-113 parameters using modern tools.

The main purpose of this work is to provide theoretical infrared spectroscopic properties of the two conformers of CFC-113 and to determine whether those results are in good agreement with experimental data. The calculations are performed by density functional theory using the Gaussian 03 software [5]. Frequency assignments and analysis of intensities are presented.

2. Computational and experimental background

Time-dependent density functional theory has become the most widely used method for determination of the molecular parameters of medium-sized molecules. It outperforms the Hartree–Fock theory by including electron correlation correction and offers an accuracy comparable to second-order Møller–Plesset theory (MP2) at a considerably lower computational cost. We are thus able to use a large basis set, including the diffuse polarization functions. The 6-311+G(3df) basis set represents a good compromise between accuracy and computational cost (only one set of diffuse and polarization functions is required as CFC-113 does not contain any hydrogen bonds). We used the well-known Becke's three-parameter exchange functional coupled with the non-local correlation from the Lee, Yang, and Parr functional (B3LYP). This recognized hybrid functional is probably the most widely used and remains the standard reference in DFT calculation [6]. The geometry optimizations and harmonic vibrational frequencies calculation are carried out simultaneously with B3LYP/6-311+G(3df).

Our theoretical results have been compared to experimental data taken in our laboratory by absorption Fourier transform infrared (FTIR) spectroscopy. The spectrometer is a Bomem DA8.002 equipped with a KBr beamsplitter and operating with a Globar source. A 25-cm-long stainless steel gas cell, mounted with ZnSe windows, is positioned between the spectrometer and a MCT (mercury–cadmium–telluride) detector. To remove non-linear Beer–Lambert effects on strong bands, an extrapolation to 0-torr (the optically thin limit) is performed from acquisitions taken at pressures varying from 0.2 to 2 torr.

3. Structure and enthalpy of the two CFC-113 conformers

CFC-113 has two geometrical conformations related to each other by a rotation of about 120° around the C–C single bond as illustrated in Fig. 1. One of the conformers, characterized by a *trans* position of two C–Cl and C–F bonds, has a C_1 symmetry while the other one, characterized by a *gauche* position of all the C–Cl and C–F bonds, has a C_s symmetry.

The results of our geometrical optimization for both conformers are presented in Table 1. The distances between
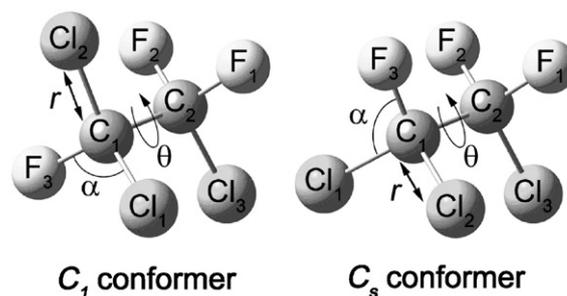
Fig. 1. The two geometrical conformations of CFC-113. *r* represents the interatomic distance (in Å); α, the angle between adjacent bonds; and θ, the dihedral angle (both in degree).

Table 1
Calculated structural parameters of the two CFC-113 conformers

	C_1 conformer	C_s conformer
$r(C_1,C_2)$	1.57	1.57
$r(C_1,F_3)$	1.34	1.35
$r(C_1,Cl_1)$	1.77	1.77
$r(C_1,Cl_2)$	1.78	1.77
$r(C_2,F_1)$	1.33	1.34
$r(C_2,F_2)$	1.34	1.34
$r(C_2,Cl_3)$	1.77	1.77
$\alpha(C_2,C_1,F_3)$	107.97	106.22
$\alpha(C_2,C_1,Cl_1)$	111.01	110.88
$\alpha(C_2,C_1,Cl_2)$	109.19	110.88
$\alpha(F_3,C_1,Cl_1)$	109.30	108.63
$\alpha(F_3,C_1,Cl_2)$	108.68	108.63
$\alpha(Cl_1,C_1,Cl_2)$	110.62	111.41
$\alpha(C_1,C_2,F_1)$	109.78	108.24
$\alpha(C_1,C_2,F_2)$	108.56	108.24
$\alpha(C_1,C_2,Cl_3)$	111.76	113.42
$\alpha(F_1,C_2,F_2)$	108.32	107.74
$\alpha(F_1,C_2,Cl_3)$	109.62	109.51
$\alpha(F_2,C_2,Cl_3)$	108.71	109.51
$\theta(F_3,C_1,C_2,F_1)$	180.00	58.22
$\theta(F_3,C_1,C_2,F_2)$	61.76	−58.30
$\theta(F_3,C_1,C_2,Cl_3)$	−58.14	179.96
$\theta(Cl_1,C_1,C_2,F_1)$	−60.21	176.06
$\theta(Cl_1,C_1,C_2,F_2)$	−178.45	59.54
$\theta(Cl_1,C_1,C_2,Cl_3)$	61.65	−62.20
$\theta(Cl_2,C_1,C_2,F_1)$	62.01	−59.63
$\theta(Cl_2,C_1,C_2,F_2)$	−56.23	−176.14
$\theta(Cl_2,C_1,C_2,Cl_3)$	−176.13	62.12

Interatomic distances (*r*) are in Å, angles (α) and dihedral angles (θ) in degrees. The position of atoms is given in Fig. 1.

the atoms are little affected by the conformational symmetry, with a C–C distance of 1.57 Å, and average C–Cl and C–F distances of 1.77 and 1.34 Å, respectively, for both configurations. We can note that the C_s conformation presents a more symmetrical structure, with identical angles and distances on the C–Cl bonds of the CFCl$_2$ group and C–F bonds of the CF$_2$Cl group.

We calculated an enthalpy difference between the two conformers of 133.6 cm^{-1}, with the C_1 structure being the more stable form. This value is in the range of those obtained by electron diffraction (94.5 ± 87.8 cm^{-1} [7])

and IR spectroscopy (122.0 ± 52.7 cm^{-1} [8]), but higher than the one obtained by matrix isolation studies (88.6 ± 9.2 cm^{-1} [4]). The predominance of the C_1 conformers can be explained by a dipole repulsion between the polar C–Cl bonds in the C_s conformation, the covalent radii of chlorine atoms being larger than those of fluorine atoms.

The transitions between the different conformations are presented in Fig. 2. To rotate from a C_1 to a C_s conformation, a molecule has to pass through the metastable eclipsed form E_1. The rotational barrier between the C_1

and C_s conformation has been calculated to be 2467.4 cm^{-1} which should make conformational interconversion difficult at room temperature. 2467.4 cm^{-1} is indeed at a higher frequency than the fundamental bands and does not correspond to the center of overtone or combination bands.

A double rotation around the C–C axis gives a statistical weight of two C_1 for one C_s conformation. The rotational barrier between the two identical C_1 conformations has been calculated as 2010.6 cm^{-1}. The energy difference between the $C_1 \leftrightarrow C_s$ (E_1) and the $C_1 \leftrightarrow C_1$ (E_2) conformational transitions may also be attributed to dipole repulsions between the polar C–Cl bonds as they approach each other in the metastable eclipsed form E_1 (see Fig. 2).

The results of the harmonic frequency calculation and vibrational assignments of the C_1 and C_s conformers are presented in Table 2. We have applied the same labeling as Braathen et al. [4] for the C_1 conformer. However we

Fig. 2. (Top) Newman projections of the stable C_1 and C_s conformers and the eclipsed metastable E_1 and E_2 structures. (Bottom) Corresponding enthalpy differences of the stable and metastable structures relatively to the lowest energy structure (C_1 conformer) as a function of the dihedral angle. Only the maxima and minima correspond to calculated values as the line has been drawn for illustration purpose only.

Fig. 3. Absorption spectrum of pure CFC-113 (Sigma–Aldrich, 99%) vapour at room temperature in the 500–1300 cm^{-1} region for a resolution of 0.5 cm^{-1}. The composite spectrum is a point-by-point extrapolation at the 0-torr limit of spectrum taken at pressures varying from 0.2 to 2.0 torr with an increment of 0.2 torr.

Table 2
Calculated vibrational frequencies (in cm^{-1}) of the two CFC-113 conformers and their description

C_1 conformation			C_s conformation		
No.	Frequency	Approximate description	No	Frequency	Approximate description
ν_1	1192.9037	C–C stretch, C–F sym. stretch	ν'_1	1187.2841	C–C stretch, C–F sym. stretch
ν_2	1163.4890	C–F asym. stretch (CF$_2$Cl)	ν'_2	1147.7966	C–F asym. stretch (CF$_2$Cl)
ν_3	1107.8234	C–F stretch (CFCl$_2$)	ν'_3	1082.2878	C–F stretch (CFCl$_2$)
ν_4	1017.4992	C–C stretch, C–F, C–Cl sym. stretch	ν'_4	1012.5698	C–C stretch, C–F, C–Cl sym. stretch
ν_5	872.4032	C–Cl asym. stretch (CFCl$_2$)	ν'_6	871.2554	C–Cl sym. stretch
ν_6	788.8769	C–Cl stretch	ν'_5	868.3722	C–Cl asym stretch (CFCl$_2$)
ν_7	651.9827	CF$_2$ scissor	ν'_7	628.6155	CF$_2$ scissor
ν_8	529.5613	CFCl$_2$ sym. deformation	ν'_9	501.6324	C–Cl sym. stretch (CFCl$_2$)
ν_9	452.3176	C–Cl sym. stretch (CFCl$_2$)	ν'_{12}	450.6277	C–Cl asym. stretch (CFCl$_2$)
ν_{10}	432.3373	C–Cl stretch (CF$_2$Cl)	ν'_{10}	432.1692	C–Cl stretch (CF$_2$Cl)
ν_{11}	389.1549	C–Cl asym. stretch (CFCl$_2$)	ν'_{11}	379.0760	C–Cl asym. stretch (CFCl$_2$)
ν_{12}	349.2677	CFCl$_2$, CF$_2$Cl asy. deformation	ν'_8	369.3358	CFCl$_2$, CF$_2$Cl sym. deformation
ν_{13}	312.2931	F–C–C bend	ν'_{13}	308.3451	CF$_2$ twist
ν_{14}	285.1914	CCl$_2$ scissor	ν'_{15}	303.8128	F–C–C bend
ν_{15}	237.4913	Cl–C–C–Cl bend	ν'_{14}	249.7756	CCl$_2$ scissor
ν_{16}	198.0344	CFCl$_2$, CF$_2$Cl rock	ν'_{17}	177.1429	CCl$_2$, CF$_2$ twist
ν_{17}	161.2550	CCl$_2$, CFCl twist	ν'_{16}	166.3632	CFCl$_2$, CF$_2$Cl rock
ν_{18}	69.1402	CFCl$_2$–CF$_2$Cl torsion	ν'_{18}	73.3685	CFCl$_2$–CF$_2$Cl torsion

Table 3
Comparison between theoretical and experimental harmonic frequencies (Freq.) given in cm^{-1} and intensities (Int.) given in 10^{-18} cm/molecule

Vibration No.	Theory				Experience	
	C_1 conformation		C_s conformation		Freq.	Int.
	Freq.	Int.	Freq.	Int.		
v_8'	—	—	501.72	0.67	n.o.	n.o.
v_8	529.56	0.4	—	—	{ 532.6 Q / 539.2 R	0.2
v_7'	—	—	628.61	2.75	{ 627.2 P / 632.7 Q / 638.4 R	0.4
v_7	651.98	1.63	—	—	{ 648.5 P / 653.7 Q / 659.5 R	1.3
v_6	788.88	47.96	—	—	815.7	28.7
v_5'	—	—	868.17	38.72		
v_6'	—	—	871.40	23.42	909.8	32.2
v_5	872.40	25.79	—	—		
v_4'	—	—	1012.91	44.16	1045.5	17.0
v_4	1017.50	13.43	—	—		
v_3'	—	—	1082.58	1.34	n.o.	n.o.
v_3	1107.82	25.86	—	—	{ 1112.2 P / 1118.4 Q / 1124.0 R	17.9
v_2'	—	—	1147.29	21.85	1171.7	21.8
v_2	1163.49	31.24	—	—	1179.8	
v_1'	—	—	1187.60	27.92	1212.7	10.5
v_1	1192.90	9.42	—	—		

n.o., non observable band.

have changed the labeling for the C_s conformer to reflect the correspondence between similar sets of nuclear displacement in the C_1 and C_s conformers.[2]

4. Frequency assignments

From the 18 normal modes of vibration of each CFC-113 conformer, only eight transitions belong to the atmospheric window, i.e. from 500 to 1300 cm^{-1}. All the transitions above 700 cm^{-1} correspond to stretching vibrations. A composite survey spectrum in the 500–1300 cm^{-1} region is presented in Fig. 3.

Due to the band broadening of CFC-113 at room temperature, the experimental harmonic frequencies presented in Table 3 have been interpolated from the barycenter of the lines. Despite the temperature broadening, we observe a good agreement between our data and those obtained at lower temperature by Braathen et al. [4].

The calculated frequencies need to be re-scaled to eliminate systematic errors [5]. Agreement between theory and experiment is very good (see Fig. 4) with a linear expression $v_{exp} = 1.02\, v_{theo} + 3.30$ (with v being the wavenumber in cm^{-1}) for the C_1 conformation and $v_{exp} = 1.03 v_{theo} - 11.08$ for the C_s conformation. The correlation coefficient R is 0.9998 for both groups.

The band around 650 cm^{-1}, corresponding to the v_7 and v_7' harmonic frequencies, is the only one where the two conformer signatures are relatively well separated (see Fig. 6). Three distinct lines, attributed to the rovibrational fundamental PQR-branches, are visible for both conformers. The PQR-branches are also found in the v_3 harmonic transition of the C_1 conformation. The same phenomenon is present around 530 cm^{-1} but the MCT detector limitation prevents access to a better signal-to-noise ratio in this region. At first sight, the v_2 and v_2' structure also seems to present PQR-branches with three distinctive lines. But all those lines have been interpreted as Q-branches as they remain in the IR spectrum of liquid CFC-113 [4]. Specifically, the interpretation of the unassigned 1187.3 cm^{-1} line is still open to discussion. The other transitions are too overlapped to allow the identification of rovibrational compounds. The structure around 977 cm^{-1} has been attributed to combination bands [8].

Beyond 1200 cm^{-1}, overtone and combination bands having intensities 2–3 orders of magnitude lower than those

---

[2] In the labeling used by Braathen et al. [4], the harmonic frequencies of the C_s conformation are numbered depending on their polarization (11a′ and 7a″). As a result, for instance, the v_2 corresponding to a C–F asymmetric stretch in the C_1 conformation becomes v_{12}' in the C_s conformation even if it corresponds to the same motion. Therefore, we modified the labeling of each C_s harmonic frequency to match the corresponding C_1 one.
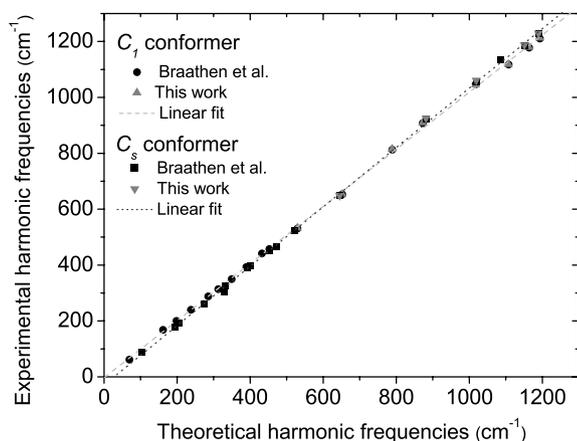
Fig. 4. Comparison between experimental and theoretical harmonic frequencies of CFC-113 for the two conformers.
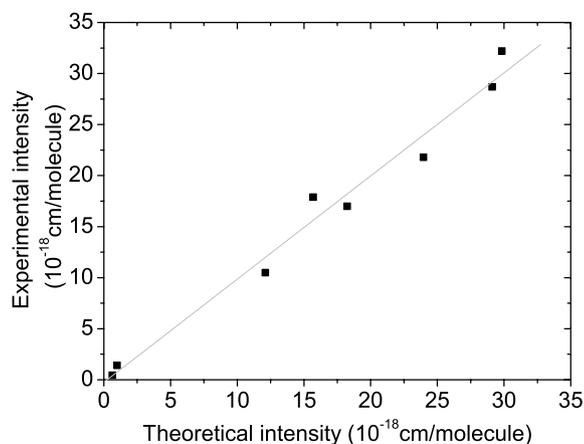
Fig. 5. Comparison between experimental and theoretical intensities of CFC-113.
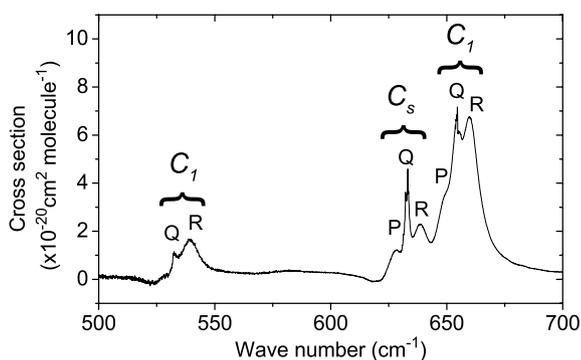
Fig. 6. Absorption spectrum of CFC-113 in the 500–700 cm^{-1} region at a pressure of 20 torr and a temperature of 10 °C for a resolution of 0.2 cm^{-1}.

of the harmonic frequencies are observed (see Fig. 7). An interpretation of those bands is given in Table 4. Two experimental bands are not assigned. It is unlikely that they correspond to impurities as they also appear in the PNNL Quantitative Infrared Database [9]. Other bands do not correspond exactly to the center of combination bands and their interpretation should include higher-order anharmonic effects such as Fermi and Coriolis resonances.
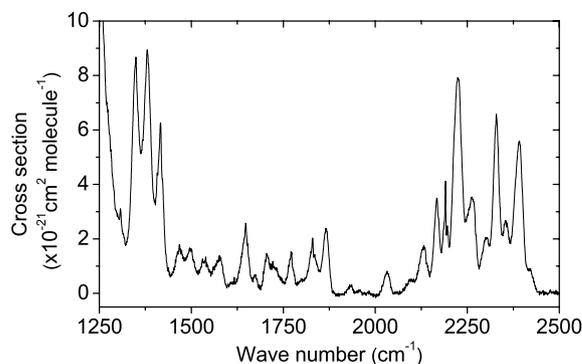
Fig. 7. Absorption spectrum of CFC-113 in the 1250–2500 cm^{-1} region at a pressure of 20 torr and a temperature of 10 °C for a resolution of 0.2 cm^{-1}.

Table 4
Assignation of the experimental overtone and combination bands in the 1200–2500 cm^{-1} region

Frequency	Intensity[a]	Interpretation[b]
2421	m	$2\nu_1$, $2\nu_1'$
2391	vs	$\nu_1 + \nu_2$, $\nu_1' + \nu_2'$
2358	m	$2\nu_2$
2329	vs	$\nu_1 + \nu_3$, $\nu_1' + \nu_3'$, $(2\nu_2')$
2301	m	$\nu_2 + \nu_3$, $(\nu_2' + \nu_3')$
2261	s	$\nu_1 + \nu_4$, $\nu_1' + \nu_4'$
2225	vs	$\nu_2 + \nu_4$, $\nu_2' + \nu_4'$, $(2\nu_3)$, $(2\nu_3')$
2195	s	?
2190	s	?
2167	s	$\nu_3 + \nu_4$, $\nu_3' + \nu_4'$
2131	m	$(\nu_1 + \nu_5)$, $(\nu_1' + \nu_6')$
2095	w	$2\nu_4$, $\nu_2 + \nu_5$, $\nu_1' + \nu_5'$, $(\nu_2' + \nu_6')$
2032	m	$\nu_3 + \nu_5, \nu_1 + \nu_6$, $\nu_3' + \nu_6'$
1957	vw	$\nu_4 + \nu_5$, $\nu_4' + \nu_6'$
1934	w	$\nu_3 + \nu_6$, $\nu_4' + \nu_5'$
1866	m	$\nu_1 + \nu_7$, $\nu_4 + \nu_6$
1830	m	$\nu_2 + \nu_7$, $(2\nu_5)$, $(2\nu_6')$
1801	w	$\nu_2' + \nu_7'$
1792	vw	$\nu_6' + \nu_5'$
1771	m	$\nu_3 + \nu_7$, $2\nu_5'$
1750	vw	$\nu_3' + \nu_7'$
1721	m	$\nu_5 + \nu_6$, $\nu_1' + \nu_9'$, $(\nu_1 + \nu_8)$
1706	m	$(\nu_2 + \nu_8)$, $(\nu_4 + \nu_7)$
1673	w	$(\nu_2' + \nu_9')$, $(\nu_4' + \nu_7')$
1648	m	$\nu_3 + \nu_8$, $(2\nu_6)$, $(\nu_3' + \nu_9')$
1579	m	$\nu_4 + \nu_8$, $(\nu_5 + \nu_7)$, $(\nu_4' + \nu_9')$
1538	m	$\nu_6' + \nu_7'$
1497	m	$(\nu_5' + \nu_7'?)$
1468	m	$\nu_6 + \nu_7$
1416	vs	$\nu_6' + \nu_9'$
1380	vs	$(\nu_5' + \nu_9')$
1348	vs	$\nu_6 + \nu_8$
1307	m	$2\nu_7$
1253	vvs	$(2\nu_7')$

[a] *Abbreviations:* s, strong; m, medium; w, weak; v, very.
[b] The harmonic frequencies in parenthesis indicate combination bands which do not correspond exactly to the barycenter of the experimental band but can be overlapped inside it.

5. Comparison between theoretical and experimental intensities

The overlapping bands of the two conformers complicate the comparison process and the calculation of the inte-

grated cross sections. The experimental and theoretical integrated cross sections in the 500–1250 cm^{-1} region are presented in Table 3. Only the v_3, v_6, v_7 and v_7' harmonic frequencies are relatively isolated. We performed a least squares fitting to determine the ratio $(C_1)/(C_s)$ which minimizes the error in the system $AX = B$ in which A represents the matrix associated with the theoretical results, X, the proportion of each group, and B, the integrated cross sections of the structures of the experimental spectrum. The structures around 530 cm^{-1} at the range limit of our detector are excluded from the calculation because of the uncertainties associated with their integrated cross-sections. The result of the least squares fitting, having a correlation coefficient of 0.9827, is presented in Fig. 5. A large part of the errors may be associated with the presence of overtones or combination bands (similar to the one at 970 cm^{-1}) overlapped in the harmonic frequencies bands.

We found a linear expression $I_{exp} = 0.61 I_{theo}(C_1) + 0.23 I_{theo}(C_s)$. The sum of the fraction of the two groups is not equal to unity. This can be explained by the fact that only the ratio between the calculated intensities have a qualitative value. The resulting percentage of C_1 conformers at room temperature, is 73%.

On another hand, considering that the statistical weight between the C_1 and C_s conformer is 2 for 1 (two over three C–C rotations results in a C_1 conformer) and applying the Boltzmann distribution for a potential energy difference of 133.6 cm^{-1}, we found a theoretical percentage of C_1 conformers of 79% at room temperature. If we use the experimental potential energy difference found by Braathen et al. [4], we obtain a percentage of C_1 conformers of about 75%.

The explanation of those differences is not obvious. Besides errors induced by the chosen theoretical method, the absence of well separated lines and possible remaining non-linear effects in the strongest lines of the experimental spectrum could explain, in part, the discrepancy in the percentage calculation. The variation of the conformer population with temperature are currently under investigation. Possible temporal or surface effects are also being considered.

6. Conclusions

A geometry optimization and a harmonic vibrational frequency calculation for CFC-113 by the density functional theory have been performed. Comparison between the theoretical harmonic frequencies and the experimental spectra show a excellent correlation. PQR structures have been identified for the v_7, v_7' and v_3 harmonic frequencies. The uncertainty in the conformers population has been pointed out. Further studies are underway in order to understand the dependence of the CFC-113 conformers' absorption spectra on temperature and pressure. The importance of this study lies in the need of precise cross-section measurement over a large range of temperature. N_2-broadening experiments are planned to evaluate the broadening effects on the rovibrational structures. Ultimately, our goal is to provide accurate IR cross section spectra to improve the retrieval of atmospheric profiles of CFC-113.

References

[1] P. Bernath, C. McElroy, M. Abrams, C. Boone, M. Butler, C. Camy-Peyret, M. Carleer, M. Clerbaux, P.-F. Coheur, R. Colin, P. DeCola, M. DeMaziere, J. Drummond, D. Dufour, W. Evans, H. Fast, D. Fussen, K. Gilbert, D. Jennings, E. Llewellyn, R. Lowe, E. Mahieu, J. McConnell, M. McHugh, S. McLeod, R. Michaud, C. Midwinter, R. Nassar, F. Nichitiu, C. Nowlan, C. Rinsland, Y. Rochon, N. Rowlands, K. Semeniuk, P. Simon, R. Skelton, J. Sloan, M.-A. Soucy, K. Strong, P. Tremblay, D. Turnbull, K. Walker, I. Walkty, D. Wardle, V. Wehrle, R. Zander, J. Zou, Geophysical Research Letters 32 (2005) L15S01.
[2] G. Dufour, C.D. Boone, F. Bernath, Geophysical Research Letters 32 (2005) L15S09.
[3] B. Sen, G.B. Osterman, R. Salawitch, G. Toon, J. Margitan, J.F. Blavier, A.Y. Chang, R.D. May, C.R. Webster, R.M. Stimpfle, G.P. Bonne, P.B. Voss, K.K. Perkins, J.G. Anderson, R.C. Cohen, J.W. Elkins, G.S. Dutton, D.F. Hurst, P.A. Romashkin, E.L. Atlas, S.M. Schauffler, M. Loewenstein, Journal of Geophysical Research 104 (1999) 26653–26665.
[4] G.O. Braathen, A. Gatial, P. Klaeboe, Journal of Molecular Structure 157 (1987) 73–91.
[5] M.J. Frisch, G.W. Trucks, H.B. Schlegel, G.E. Scuseria, M.A. Robb, J.R. Cheeseman, J.A. Montgomery, Jr., T. Vreven, K.N. Kudin, J.C. Burant, J.M. Millam, S.S. Iyengar, J. Tomasi, V. Barone, B. Mennucci, M. Cossi, G. Scalmani, N. Rega, G.A. Petersson, H. Nakatsuji, M. Hada, M. Ehara, K. Toyota, R. Fukuda, J. Hasegawa, M. Ishida, T. Naka- jima, Y. Honda, O. Kitao, H. Nakai, M. Klene, X. Li, J.E. Knox, H.P. Hratchian, J.B. Cross, V. Bakken, C. Adamo, J. Jaramillo, R. Gomperts, R. E. Stratmann, O. Yazyev, A.J. Austin, R. Cammi, C. Pomelli, J.W. Ochterski, P.Y. Ayala, K. Morokuma, G.A. Voth, P. Salvador, J.J. Dannenberg, V.G. Zakrzewski, S. Dapprich, A.D. Daniels, M.C. Strain, O. Farkas, D.K. Malick, A.D. Rabuck, K. Raghavachari, J.B. Foresman, J.V. Ortiz, Q. Cui, A.G. Baboul, S. Clifford, J. Cioslowski, B.B. Stefanov, G. Liu, A. Liashenko, P. Piskorz, I. Komaromi, R.L. Martin, D.J. Fox, T. Keith, M.A. Al-Laham, C.Y. Peng, A. Nanayakkara, M. Challacombe, P.M., Gaussian 03, Revision C.02, Gaussian, Inc., Wallingford, CT, 2004.
[6] A. Boese, J. Martin, N. Handy, Journal of Chemical Physics 119 (2003) 3005.
[7] M. Iwasaki, Bulletin of the Chemical Society of Japan 32 (1959) 205–214.
[8] P. Klaboe, J. Rud Nielsen, Journal of Molecular Spectroscopy 6 (1961) 79–393.
[9] Pacific Northwest National Laboratory (PNNL) Quantitative Infrared Database, available online at https://secure2.pnl.gov/nsd/nsd.nsf/Welcome.